applied sciences

MDPI

Article

Spindle Thermal Error Prediction Based on LSTM Deep Learning for a CNC Machine Tool

Yu-Chi Liu [1,*], Kun-Ying Li [2] and Yao-Cheng Tsai [1]

[1] Department of Computer Science and Information Engineering, National Chin-Yi University of Technology, Taichung 411030, Taiwan; s4a917017@student.ncut.edu.tw
[2] Graduate Institute of Precision Manufacturing, National Chin-Yi University of Technology, Taichung 411030, Taiwan; likunying@ncut.edu.tw
* Correspondence: ycliu@ncut.edu.tw

Abstract: In the precision processing industry, maintaining the accuracy of machine tools for an extensive period is crucial. Machining accuracy is affected by numerous factors, among which spindle thermal elongation caused by an increase in machine temperature is the most common. This paper proposed a key temperature point selection algorithm and thermal error estimation method for spindle displacement in a machine tool. First, highly correlated temperature points were clustered into groups, and the characteristics of small differences within groups and large differences between groups were realized. The optimal number of key temperature points was then determined using the elbow method. Meanwhile, the long short-term memory (LSTM) modeling method was proposed to establish the relationship between the spindle thermal error and changes of the key temperature points. The results show the largest root mean square errors (RMSEs) of the proposed LSTM model and the key temperature point selection algorithm were within 0.6 μm in the spindle thermal displacement experiments with different temperature changes. The results demonstrated that the combined methodology can provide improved accuracy and robustness in predicting the spindle thermal displacement.

Keywords: spindle thermal error; elbow method; long short-term memory (LSTM)

Citation: Liu, Y.-C.; Li, K.-Y.; Tsai, Y.-C. Spindle Thermal Error Prediction Based on LSTM Deep Learning for a CNC Machine Tool. *Appl. Sci.* **2021**, *11*, 5444. https://doi.org/10.3390/app11125444

Academic Editor: Mark J. Jackson

Received: 10 May 2021
Accepted: 7 June 2021
Published: 11 June 2021

1. Introduction

The global precision machinery market has expanded and shifted its focus to high value-added products, particularly those in the spaceflight, automotive, and mold industries. The products in these industries are mostly characterized by complex structures or irregular surfaces, and are thus difficult to process. During the transformation of high value products, increasing or maintaining the machining accuracy of machine tools is essential. Researchers have indicated that the thermal deformation in precision machinery caused by the internal and external heat sources of machine tools accounts for 50–70% of total errors [1–3], making thermal deformation a major precision control problem common to all precision machinery. In order to improve the above problem, researchers have proposed using thermal stability materials to manufacture machine tools [4–7], redesign the mechanism of isolating heat sources [8] or redesign cooling channels to reduce the temperatures of heat sources [9–12]. Although these approaches effectively mitigate thermal errors, they are considerably cost intensive and cause other problems, such as increased vibration and reduced acceleration of the machine tool [13]. Therefore, mathematical prediction models of the spindle thermal displacement have been proposed to establish the temperature–spindle deformation relationship in a machine tool and to provide the basis for a controller to compensate for the thermal displacement of the spindle. Such models have become widely preferred and applied in various types of computer numeric control (CNC) machine tools, such as gantry-type machine centers [14], three-axis vertical machining centers [15], lathe machines [16] and so on. In application, the hardware module for compensation of spindle thermal error was established to collect the online temperature values from the key positions of a machine tool, calculate the compensation value using mathematical models, and communicate with the CNC controller. The axes positioning was periodically readjusted by the control of the machine tool, based on the received compensation value. Multiple linear regression (MLR) is a common algorithm for creating mathematical prediction models of thermal displacement [17–23]. Some neural network modeling techniques have also been proposed to obtain more robust and accurate predictions [24–32]. In addition, how to select and decide the representative temperature-sensitive points among numerous Initial Temperature Points (ITPs) is crucial. The performance of the selection method directly affects the accuracy of the estimation model as well as the cost of system implementation. Miao et al. [21] proposed a modeling method based on a principal component regression (PCR) algorithm, which can eliminate the influence of multi-collinearity among temperature variables. Both PCR and MLR were given practice tests through thermal error experiments of actual machine. And the results show, the model had good forecasting accuracy and robustness using the PCR model. Liu et al. [22] proposed using a fuzzy clustering algorithm to cluster highly correlated ITPs. With a gray prediction algorithm, the gray correlation between the temperature points of each group and displacements was analyzed. The temperature point with the greatest gray correlation was selected as the key temperature point (KTP) for each group. Finally, a ridge regression algorithm was proposed to establish the thermal displacement model. Liu et al. [23] presented a new thermal error modeling method called GR-SUE. In the GR-SUE method, several temperature-sensitive points with the highest-influence weights on thermal error ware directly selected using the gray relation algorithm. A split unbiased estimation modeling algorithm was subsequently proposed to improve the MLR algorithm to inhibit the influence of collinearity on model prediction accuracy and robustness. The experimental results indicated that the GR-SUE method could significantly reduce the volatility of temperature-sensitive points and improve the prediction accuracy and robustness of the model. Yin et al. [29] used the fuzzy c-means clustering algorithm to cluster ITPs and select key temperature-sensitive points. Yin et al. also adopted a genetic algorithm to optimize a BackPropagation neural network (BPNN) to reduce the instability of the thermal displacement estimation models. Zhou et al. [30] established a total of 222 ITPs from different structural positions of a machine tool; among the ITPs, KTPs were selected using density-based clustering. Subsequently, a steepest descent algorithm was replaced by the genetic algorithm in a BPNN to establish a thermal displacement model. Lou et al. [31] analyzed 27 ITPs and displacement stability by using the ratio of temperature variations to displacement variations over time. Highly correlated ITPs were clustered using a fuzzy clustering algorithm, and the KTPs with the greatest stability for each cluster were defined. Finally, a BPNN was used to create a thermal displacement model. The results revealed that the screened KTPs had higher estimation accuracy than did the remaining points. By performing an analysis based on the grey prediction algorithm, Abdulshahed et al. [32] analyzed the grey action values of 76 ITPs and their displacement levels, after which the fuzzy clustering algorithm was used to cluster these values for KTP selection. Finally, the adaptive neuro-fuzzy inference system was adopted to establish a spindle thermal displacement model. The results demonstrated that the root mean square errors (RMSEs) of the proposed model were within 4 μm in thermal error experiments with different temperature increases and decreases.

The aforementioned studies have demonstrated that appropriate KTP selection and the use of highly accurate and robust estimation models are necessary for the improvement of spindle thermal errors in machine tools. In the present study, several ITPs were defined according to an analysis of machine tool structures, experience, and internal and external heat sources. Subsequently, the spindle thermal displacement experiments were conducted to measure both the temperatures of all the ITPs and the spindle displacement in the z-direction for different spindle rotation speeds. After the experimental data were collected, a reference point for temperature increase was obtained by calculating the variance for each ITP. Highly correlated ITPs were then clustered, and the elbow method [33] was adopted to determine the optimal number of KTPs. Finally, according to the characteristics of the data, an artificial neural network (ANN) using long short-term memory (LSTM) architecture was designed to establish a spindle thermal displacement model in the z-direction. This model can be used as the basis for the spindle thermal displacement compensation in a machine tool to maintain machining accuracy.

2. Materials and Methods

The proposed method included ITP analysis, experimental design to obtain experimental data, temperature increase reference point analysis, ITP clustering, KTP selection, data normalization, and the establishment of the thermal displacement model of the spindle in the z-direction. The flowchart of the proposed method is shown in Figure 1. In Table A1, the notations of all the symbols and variables used are summarized in this paper.

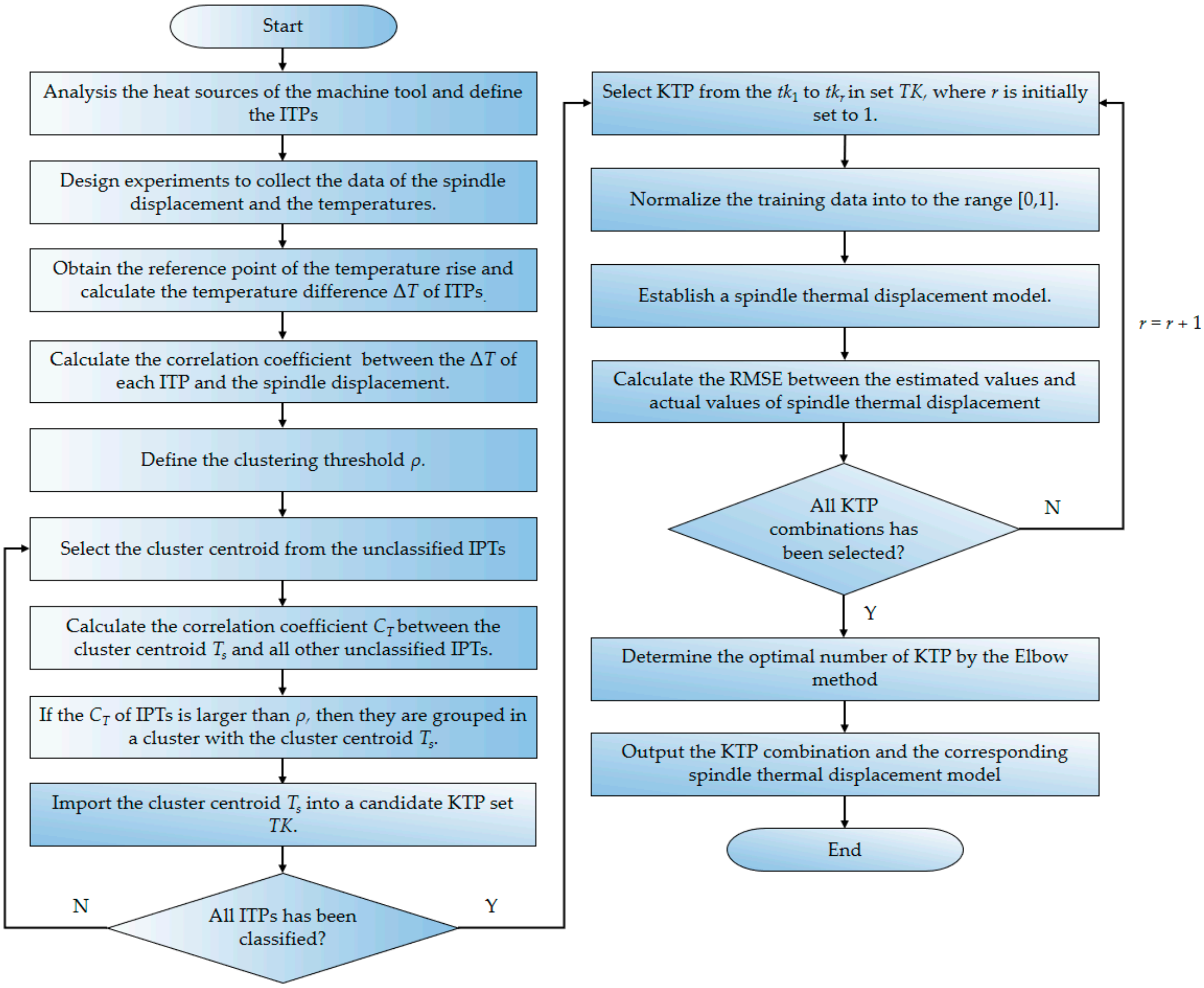

Figure 1. The flowchart of the proposed method.

2.1. ITP Analysis and Experimental Design

Spindle thermal displacement in a machine tool is mainly caused by the expansion of metal parts in response to internal and external heat sources. When the spindle starts to rotate at high speed, mechanical friction occurs between the spindle motor, bearing, and gear, producing thermal energy. These resultant internal heat sources transfer heat through conduction to the spindle part and the ambient casting parts. The temperature of these casting parts increases, resulting in heat deformation [13]. In addition, external heat sources (i.e., environmental temperature and sunlight) indirectly affect casting part temperature through heat radiation [13]. By considering the heat sources, machine tool structures, and experience, n ITPs $T = \{T_1, T_2, \ldots, T_n\}$ can be selected. Meanwhile, three thermal error experiments with low, moderate, and high machine tool rotation speeds were separately conducted. For example, because the maximum rotation speed of the spindle is 10,000 rpm, three spindle thermal error experiments were planned at three rotation speeds: 3000, 6000, and 9000 rpm. The machine tool was run for 8 h at each speed level and stopped for another 8 h for cooling, enabling the identification of structural deformations. For each experiment, the spindle thermal error was measured in accordance with the "five-point method" from the international standard "Test code for machine tools—Part 3: Determination of thermal effects" (ISO 230-3:2001 IDT) [34]. Specifically, five Omron ZX-EM02T [35] eddy current noncontact displacement sensors were installed, along with a test bar, to simulate the cutting points of the machine tool, as illustrated in Figure 2. The specifications of the MISUMI NT50-CMA30-225 (Ikoma, Japan) test bar [36] are shown in Figure 3. Online data of the spindle displacement in the z-direction E were sampled at a frequency of 30 s.

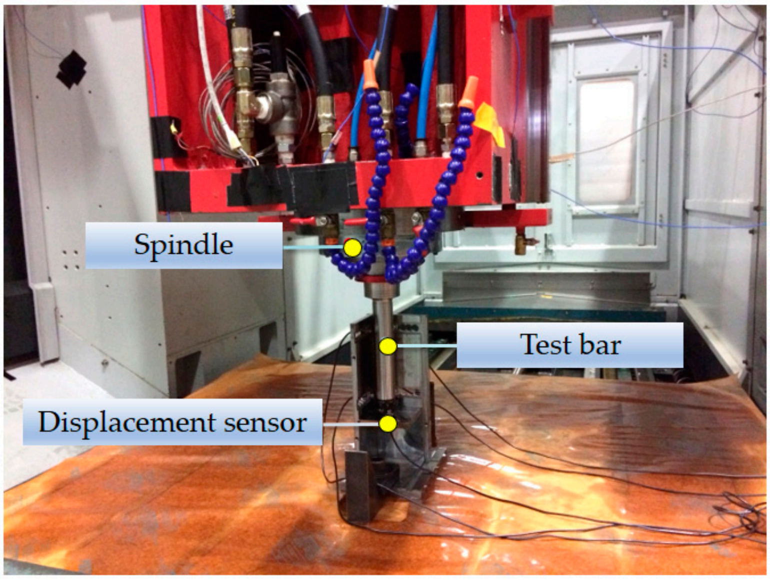

Figure 2. Installation description of the displacement sensor and test bar.

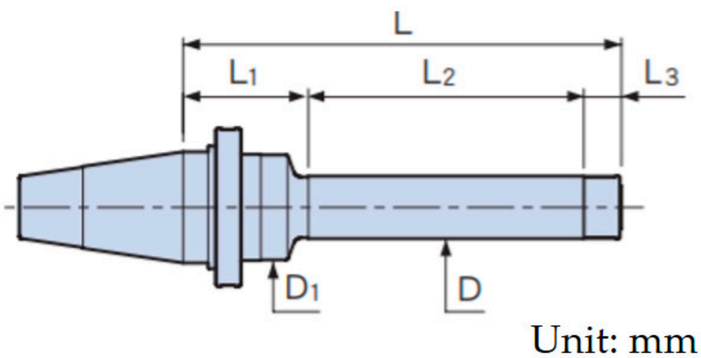

ΦD	$ΦD_1$	L	L_1	L_2	L_3
30	53	225	65	145	15

Figure 3. The specifications of the MISUMI NT50-CMA30-225 (Ikoma, Japan) test bar [36].

2.2. Analysis and Selection of the Temperature Rise Reference Point

Generally, the machining accuracy of a machine tool is affected by the environmental temperature unless it is placed in a processing environment with a constant temperature. The environmental temperature changes with the amount of sunlight, the season, and weather, creating different environmental temperature conditions at the beginning of and during machine tool processing [37]. Under such circumstances, thermal errors that occur after the machine tool has been running for a long period may have various consequences. To mitigate the effects of environmental temperature on the machine tool and obtain a stable basis for thermal error compensation, this paper aimed to identify a reference point T_b of temperature rise among the ITPs. Specifically, the variance of each ITP was calculated by Equation (1). In probability theory and statistics, variance is a statistical measurement of the spread between numbers in a data set. Variance can measure how far each number in the set is from the mean. The larger variance value, the greater the data dispersion and variation were. Conversely, a small variance value indicates slight variation. When this characteristic is used, the ITP with minimum variation after a long period of spindle operation can be identified and defined as the reference point T_b. Since T_b was excluded from the original ITPs, the number of ITPs is hereafter denoted as $n - 1$. Subsequently, the temperature difference of each ITP (except for the reference ITP) was obtained by subtracting T_b from the ITP value, which was denoted as $\Delta T = \{\Delta T_1, \Delta T_2, \ldots, \Delta T_{n-1}\}$, where $\Delta T_1 = T_1 - T_b$. These temperature differences were adopted as the basis for the subsequent spindle thermal displacement analysis, modeling, and model application.

$$SS(T) = \frac{1}{A}\sum_{a=1}^{A}\left(T_{1,a} - \overline{T_1}\right)^2, \tag{1}$$

where A denotes the number of data.

2.3. KTP Selection Method

The effectiveness of the KTP selection method affects the performance of spindle thermal displacement modeling and the cost of system implementation. Excessive temperature points cause overfitting in ANN learning, consequently reducing the predictive ability of the model. To solve the aforementioned problems, a clustering algorithm with the elbow method was proposed to determine the optimal number of KTPs in this study. This approach can effectively reduce the dimensionality of ITPs. Specifically, the Pearson correlation coefficient was used to acquire a measure of the linear correlation $C_Z(E, \Delta T)$ between the temperature difference ΔT of each ITP and the spindle displacement in the z-direction E, as expressed in Equation (2). The correlation coefficient C_T between ITPs can also be measured. In addition, the RMSE was calculated to confirm the performance of the estimation model in Equation (3). A small RMSE indicates a small difference between the actual and estimated value of spindle displacement in the z-direction E and suggests a higher predictive ability of the estimation model.

$$Cz(E, \Delta T) = \frac{\sum_{a=1}^{A}\left(\Delta T_{1,a} - \overline{\Delta T_1}\right)\left(Z_a - \overline{Z}\right)}{\sqrt{\left(\Delta T_{1,a} - \overline{\Delta T_1}\right)}\sqrt{\left(Z_A - \overline{Z}\right)}}, \tag{2}$$

$$RMSE = \sqrt{\frac{1}{A}\sum_{a=1}^{A}\left(Z_a - y_a\right)^2}, \tag{3}$$

where A denotes the number of data, E is the actual spindle displacement in the z-direction, and y represents the estimated output from the estimation model. The steps of the KTP selection method are described as follows:

Step 1: Define the clustering threshold ρ.

Step 2: Obtain the correlation coefficient $C_Z(E, \Delta T)$ between the temperature difference of each unclassified IPT, ΔT, and the actual spindle displacement in the z-direction E.
Step 3: Among the unclassified IPTs, select the temperature point that is the most correlated with the spindle thermal displacement and define it as cluster centroid T_s.
Step 4: Calculate the correlation coefficient $C_T(T_s, \Delta T)$ between cluster centroid T_s and all other unclassified IPTs, individually.
Step 5: If the correlation coefficient $C_T(T_s, \Delta T)$ of the unclassified IPTs is larger than the clustering threshold ρ, then they are grouped in a cluster with cluster centroid T_s. Meanwhile, import cluster centroid T_s into a candidate KTP set *TK*.
Step 6: Repeat Steps 3–5 until all the n–1 ITPs are grouped, resulting in the final candidate KTP set $TK = \{tk_1, tk_2, \ldots, tk_v\}$, where v denotes the total number of groups.
Step 7: In the candidate KTP set *TK*, select KTPs from tk_1 to tk_r, where r is initially set to 1. Next, establish the prediction model of the thermal displacement of the spindle, the details of which are specified in Sections 2.4 and 2.5.
Step 8: Use the data from the high-speed spindle rotation experiment to calculate the RMSE between the estimated values and actual values of spindle thermal displacement.
Step 9: Add 1 to r and repeat Steps 6 and 8 until the RMSEs are obtained for all the KTP combinations.
Step 10: Adopt the elbow method [33] to plot a graph, in which the x-axis denotes the number of KTP c and the y-axis denotes the RMSE.
Step 11: Identify where the line in a graph is curved without an obvious decrease and relate the point (i.e., the elbow of the curve) to the corresponding c value (i.e., the point where all RMSEs have nearly converged). This value c was defined as the optimal number of *KTP*s.

2.4. Definition and Normalization of the Modeling Data

Li et al. [38] mentioned that when establishing a thermal displacement model, inputting variables unrelated to temperature increase into the model (e.g., spindle rotation speed, load inertia ratio, and spindle current) can improve the predictive ability of the model. Therefore, in addition to treating the KTP combination obtained in the previous section as a model input, the model uses the spindle rotation speed S as a variable. The values of these model inputs undergo min–max normalization as expressed in Equation (4). All values were mapped to the range [0, 1] and were used as the input for model training and application.

$$d_{nom} = \frac{d - d_{\min}}{d_{\max} - d_{\min}}, \tag{4}$$

where $d_{\max}$ and $d_{\min}$ denotes the maximum and minimum value in the specified data, respectively.

2.5. Establishment of a Spindle Thermal Displacement Model in the Z-Direction

In a recurrent neural network (RNN), when a hidden layer is calculated, the output is passed back to the layer itself as an input. This approach enables the effective storage of historical information. Therefore, an RNN can more effectively predict time series data compared to a feedforward neural network. However, the conventional RNN method will cause long-term memory to be covered by short-term memory because of the mathematical vanishing gradient problem. The RNN method thus has difficulties in capturing long-term memory. Hochreiter et al. proposed the LSTM [39] to improve this RNN defect. An LSTM memory cell has several gates that can decide whether the input and output information can be stored and exported. A memory cell is mainly comprised of an input gate, a forget gate, and an output gate. The input gate determines whether the neural input in question should enter the memory cell, the forget gate decides whether the information within the cell should be eliminated, and the output gate decides whether the memory cell should be output. The updated equations for the three gates are as follows:

$$i_t = sigmoid\left(x_t U^i + h_{t-1} W^i\right) + b^i \tag{5}$$

$$f_t = sigmoid\left(x_t U^f + h_{t-1} W^f\right) + b^f \tag{6}$$

$$o_t = sigmoid(x_t U^o + h_{t-1} W^o) + b^o \tag{7}$$

$$\widetilde{c}_t = \tanh(\ x_t U^g + h_{t-1} W^g) + b^g \tag{8}$$

$$c_t = sigmoid(\ f_t \times c_t + i_t \times \widetilde{c}_t) \tag{9}$$

$$h_t = \tanh\ (c_t) \times o_t \tag{10}$$

where x_t is the input value of the t^{th} datum. Variables i_t, U^i, W^i, and b^i denote the output, input weight, previous output weight, and bias of the input gate, respectively. Variables f_t, U^f, W^f, and b^f are the output, input weight, previous output weight, and bias of the forget gate, respectively. Variables o_t, U^o, W^o, and b^o represent the output, input weight, previous output weight, and bias of the output gate, respectively. Variable $\widetilde{c}_t$ is the current neural output, while U^g is the neural input weight, W^g is the previous output weight of the neuron, b^g is the bias of the neuron, c_t is the memory cell output, and h_t is the LSTM unit output. With the three-gate mechanism, LSTM architecture can store old data on a memory cell for deep learning. This technique has advanced in fields such as text generation, machine translation, speech recognition, and image description generation. Because the data of temperature increase and spindle displacement resemble time series data, the LSTM scheme is an ideal option for modeling. In this study, LSTM modeling was adopted to create a z-direction spindle thermal displacement model to accurately estimate the spindle displacement with various rotation speeds. The temperature increase ΔT of the KTP combination and the spindle rotation speed S were the inputs, and the z-direction displacement of the spindle was the output. Based on input data complexity, the control parameters, including several hidden-layer neurons, several hidden layers, neuron bias, and nonlinear transfer functions, were designed for LSTM training. The LSTM estimation results were later compared to those of an MLR and BPNN.

3. Experimental Results

3.1. Environment Establishment and Experimental Result Analysis

In this study, an AWEA VP-2012 (Hsinchu, Taiwan) three-axis gantry-type machining center with a direct drive spindle was the experimental subject, of which the highest rotation speed is 10,000 rpm. According to the heat source and experience analytical results, a total of 47 ITPs were established in different machine structures and positions of the machine tool, as shown in Figure 4 and Table 1, respectively. In Figure 4, T_0 is defined as the origin of the mechanical coordinates for AWEA VP-2012, and the absolute Cartesian coordinates for all ITPs are shown in Table A2.

Subsequently, three spindle thermal displacement experiments were conducted in a constant temperature environment of 25 degrees. For each experiment, the spindle thermal displacement was measured in accordance with the "five-point method" from the international standard, and the details are recorded in Section 2.1. The spindle rotation speeds were set to 3000, 6000, and 9000 rpm. For each experiment, the machine was run for 8 h and turned off for another 8 h, as shown in Figure 5. The maximum spindle displacements at 3000, 6000, and 9000 rpm were −18, −39, and −65 μm, respectively. When the machine was turned off after running for 8 h hours, temporary reverse displacement of the spindle in the z-direction was observed. This phenomenon occurred because when the spindle rotation speed was switched between high rates, the resulting centrifugal force changes caused a change in the bearing load, which indirectly affected the contact angle between the inner and outer bearing rings and the balls, leading to changes in spindle displacement in the z-direction. The higher the spindle rotation speed, the greater the axial displacement.

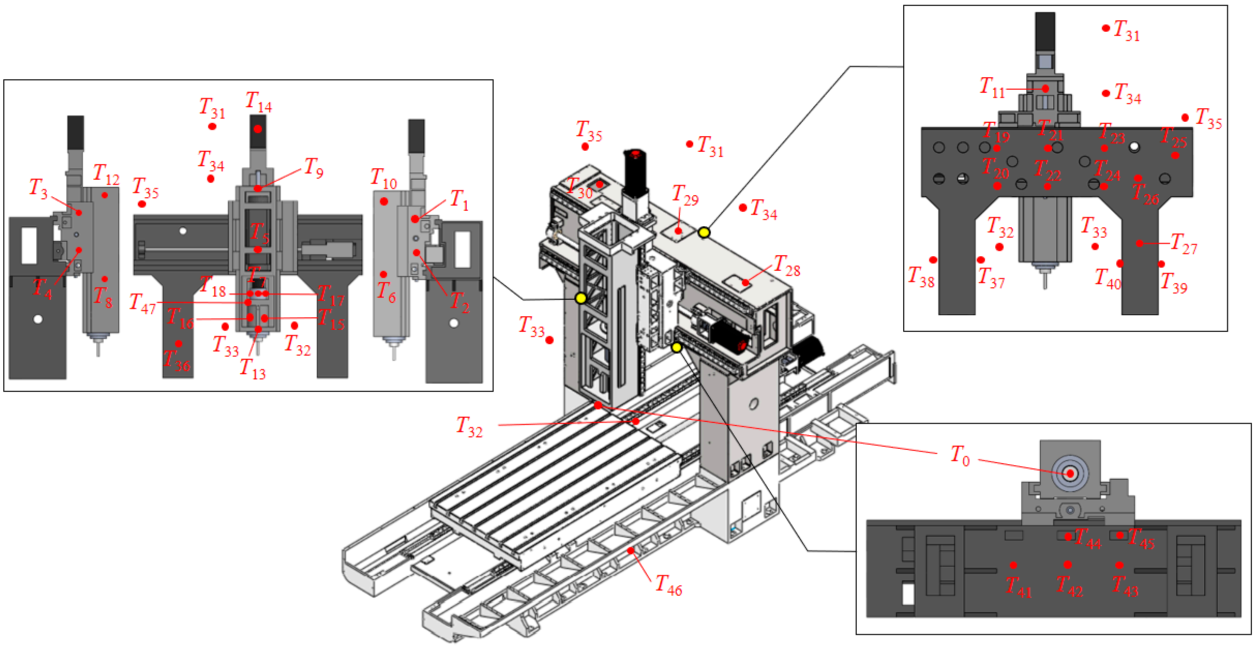

Figure 4. Positions of the 47 ITPs for AWEA VP-2012 (Hsinchu, Taiwan).

Table 1. Description of the ITPs corresponding to machine structure positions.

Position on the Machining Center	Initial Temperature Points (ITPs)
Spindle	$T_1, T_2, \ldots, T_{18}$
Behind the cross beam	$T_{19}, T_{20}, \ldots, T_{27}$
Above the cross beam	T_{28}, T_{29}, T_{30}
Environmental temperature	$T_{31}, T_{32}, T_{33}, T_{34}, T_{35}$
Column	$T_{36}, T_{37}, T_{38}, T_{39}, T_{40}$
Below the cross beam	$T_{41}, T_{42}, T_{43}, T_{44}, T_{45}$
Base	T_{46}
Oil chiller inlet	T_{47}

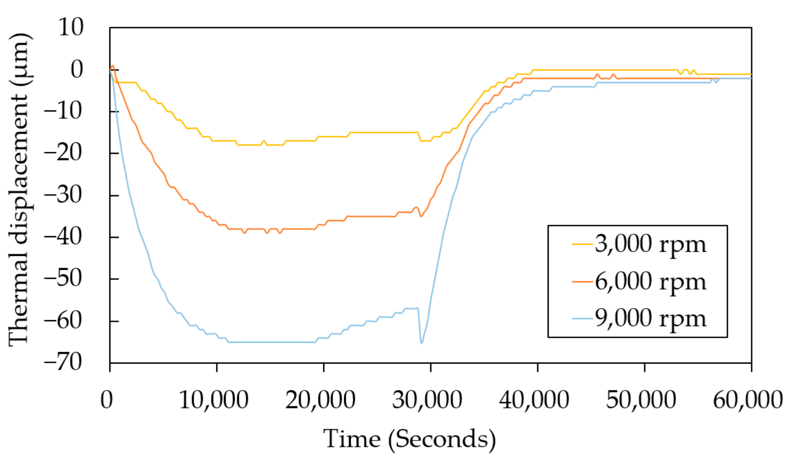

Figure 5. Spindle displacement in the z direction at different spindle rotation speeds.

To select the reference point of the temperature increase, the variance of the 47 ITPs $\boldsymbol{T} = \{T_1, T_2, \ldots, T_{47}\}$ was be calculated by using Equation (1). The resulting values were then arranged in ascending order. Table 2 lists the serial numbers of the first ten ITPs and their variance. ITP T_{46} with the smallest variance was set as the reference point T_b. Subsequently, the temperature rise of each ITP (except for the reference ITP) was obtained by subtracting the value of T_b from the ITP value in question, which is denoted as $\Delta T = \{\Delta T_1, \Delta T_2, \ldots, \Delta T_{n-1}\}$, where $\Delta T_1 = T_1 - T_b$.

Table 2. The variance of the first ten ITPs.

Temperature Point	Variance
T_{46}	0.491
T_{39}	0.532
T_{36}	0.535
T_{40}	0.573
T_{19}	0.586
T_{20}	0.591
T_{43}	0.593
T_{28}	0.596
T_{34}	0.601
T_2	0.606

At the stage of obtaining KTPs, the correlation coefficients $C_Z(E, \Delta\boldsymbol{T})$ between the temperature increase of each ITP and the spindle displacement in the z-direction E were calculated. To simplify observation, the acquired correlation coefficients were arranged in descending order, as presented in Table 3. ITP T_{17} was set as the first KTP group centroid because it had the strongest correlation with the spindle displacement. Subsequently, the correlation coefficients (C_T) between ITP T_{17} and the other 45 ITPs were determined. Table 4 presents the first ten ITPs in descending order and their corresponding correlation coefficients. The clustering threshold ρ was set to 0.9. ITPs larger than this ρ value were then grouped together. Specifically, T_5, T_6, T_7, T_8, and T_{18} were assigned to group 1, and the ITP T_{17} was the cluster centroid. The remaining ITPs were continuously analyzed according to their correlations with the spindle displacement, as shown in Table 5. Table 5 indicates that ITP T_9 was the centroid of group 2. The correlation coefficients between T_9 and the remaining ITPs were determined, as listed in Table 6. According to the clustering threshold ρ, the temperature points belonging to group 2 were then identified. These steps were repeated until all the ITPs were clustered. Finally, 13 clustering results were obtained, as shown in Table 7. Meanwhile, 13 cluster centroids were collected as candidate KTP set *TK*.

Table 3. The strongest negative correlations of five ITPs with spindle displacement.

ITP	Correlation Coefficient *Cz*
T_{17}	−0.959
T_7	−0.957
T_{18}	−0.956
T_5	−0.911
T_9	−0.890

Table 4. The ten ITPs with the strongest correlations with T_{17}.

ITP	Correlation Coefficient C_T
T_{18}	0.999
T_7	0.993
T_5	0.965
T_6	0.958
T_8	0.951
T_{15}	0.899
T_9	0.886
T_{10}	0.880
T_{16}	0.852
T_{21}	0.830

Table 5. The five ITPs with the strongest negative correlations with the spindle displacement.

ITP	Correlation Coefficient Cz
T_9	−0.890
T_{15}	−0.883
T_{10}	−0.871
T_{27}	−0.851
T_{23}	−0.842
T_{26}	−0.830
T_{14}	−0.807
T_{25}	−0.796
T_{34}	−0.788
T_{21}	−0.785

Table 6. The fifteen ITPs with the strongest correlations with T_9.

ITP	Correlation Coefficient C_T
T_{10}	0.995
T_{15}	0.993
T_{23}	0.945
T_{21}	0.943
T_{34}	0.926
T_{25}	0.922
T_{38}	0.921
T_{29}	0.920
T_{26}	0.917
T_{24}	0.909
T_3	0.908
T_{19}	0.900
T_{27}	0.898
T_{14}	0.894
T_{35}	0.888

Table 7. Final ITP clustering results.

Group	ITPs	Key Temperature Point (KTP)
1	T_5, T_6, T_7, T_8, T_{17}, T_{18}	T_{17}
2	T_3, T_9, T_{10}, T_{15}, T_{19}, T_{21}, T_{23}, T_{24}, T_{25}, T_{26}, T_{29}, T_{34}, T_{38}	T_9
3	T_{27}	T_{27}
4	T_{11}, T_{14}	T_{14}
5	T_{32}, T_{33}, T_{35}	T_{32}
6	T_{16}, T_{13}, T_{12},	T_{16}
7	T_4, T_{20}, T_{22}, T_{28}, T_{30}, T_{37}, T_{40}, T_{41}	T_{37}
8	T_1, T_2	T_1
9	T_{31}	T_{31}
10	T_{47}	T_{47}
11	T_{42}, T_{43}, T_{44}, T_{45}	T_{42}
12	T_{39}	T_{39}
13	T_{36}	T_{36}

In determining a favorable KTP combination, the x-axis and y-axis of an analysis chart were first defined as the number of KTP and the RMSE, respectively. The number of the KTP of the x-axis means that the several KTPs will be selected, in sequence, beginning from the first one in candidate KTP set TK. For example, two KTPs, T_{17} and T_9, will be picked up in order from the first one in TK when the number of KTP is 2. And, when the number of KTP is 7, seven KTPs will be selected in sequence from the first KTP in TK: T_{17}, T_9, T_{27}, T_{14}, T_{32}, T_{16} and T_{37}. In this case, 13 KTP combinations could be obtained. Placing the RMSE on the y-axis represents the predictive ability of the KTP combination using the data from the 9000 rpm spindle rotation speed rotation experiment. Meanwhile, the spindle thermal displacement model for each KTP combination was individually established by the proposed LSTM modeling method, the details of which are specified in Section 3.3. On the basis of the elbow method, the point corresponding to the elbow of the curve, with relatively convergent clusters, was identified and linked to the corresponding KTP number c on the y axis. This point represents the point where the RMSEs of all KTPs were nearly convergent, and it was thus regarded as the optimal KTP number. Figure 6 shows the RMSEs of a different number of KTPs within the LSTM model at the 9000 rpm spindle rotation speed. It indicates that a turning point occurred when the KTP number was two. When the KTP number was increased to five, the curve no longer exhibited a noticeable decrease, indicating that the optimal number of KTPs is five.

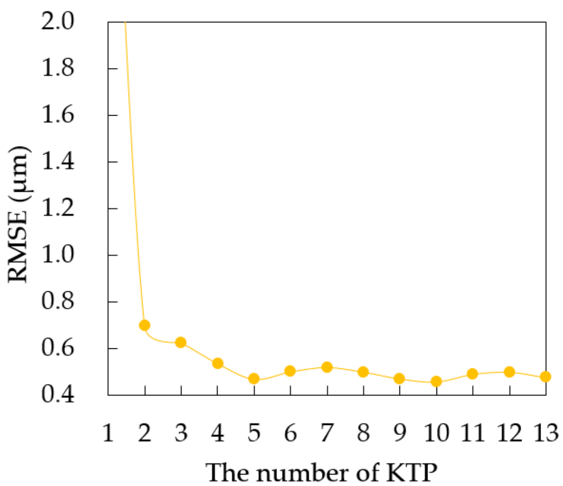

Figure 6. The root mean square errors (RMSEs) for different number of key temperature point (KTP).

3.2. Analysis of KTP Combinations

Figure 7 shows the temperature trends within the first five groups clustered by the above subsection. The proposed KTP selection method was proven to result in a small intragroup difference and large intergroup difference. Moreover, T_{17}, which was the KTP of group 1 and its group members were all distributed near the spindle motor. The temperature points of group 2 (with T_9 being the KTP) were situated above the cross beam, which was close to the spindle motor. The temperature points of group 3 (KTP = T_{27}) were located behind the cross beam on the left, close to the oil chiller. The temperature points of group 4 (KTP = T_{14}) were located on the spindle motor. Three temperature points of group 5 (KTP = T_{32}) represented the environmental temperatures below the spindle head. Figure 8 presents the trend analysis of five KTP temperatures and spindle displacement, revealing considerable differences in temperature increases among the clusters. These results indicate that the proposed KTP selection method has effective grouping ability.

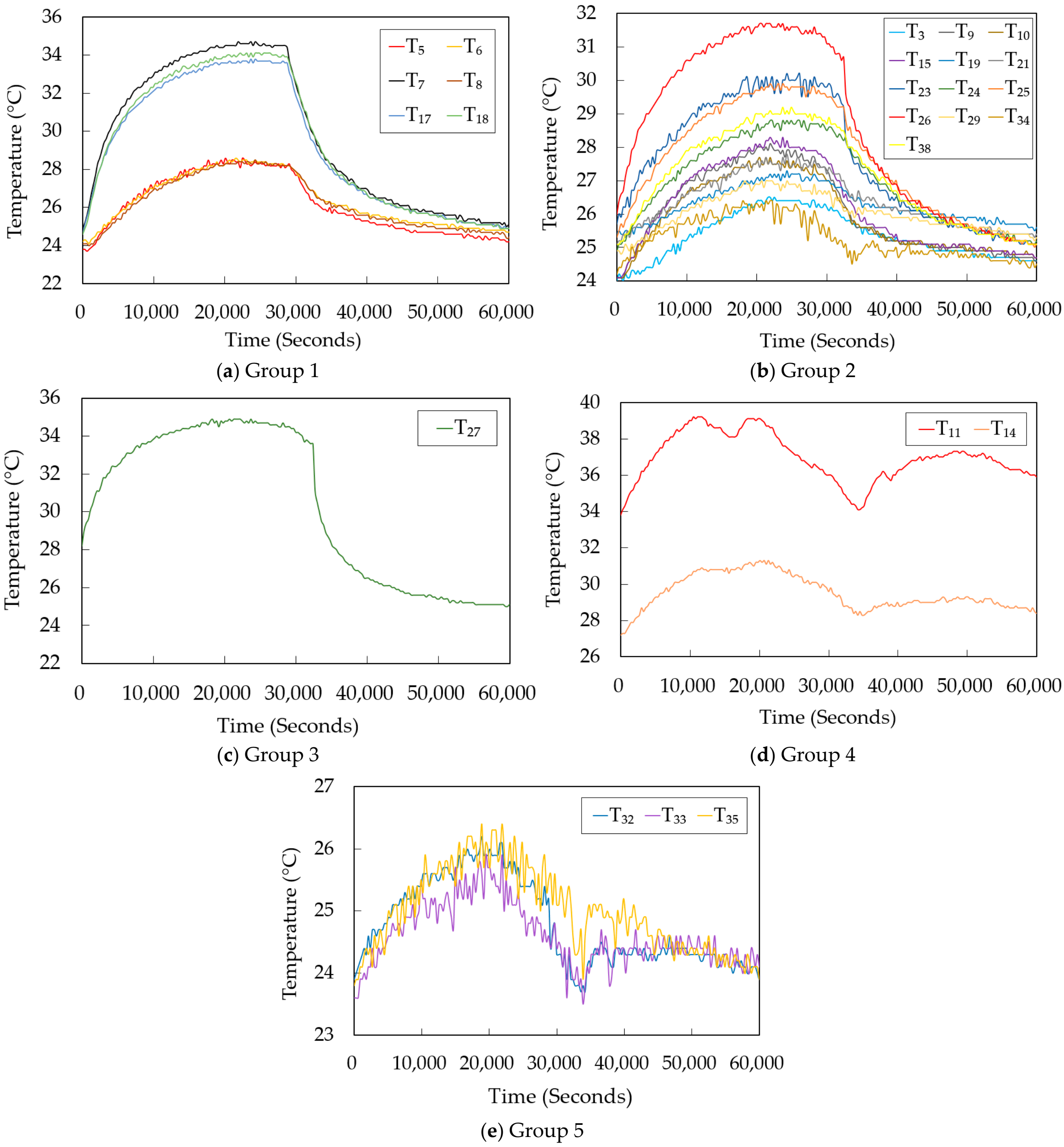

Figure 7. Temperature trends within the first five groups.

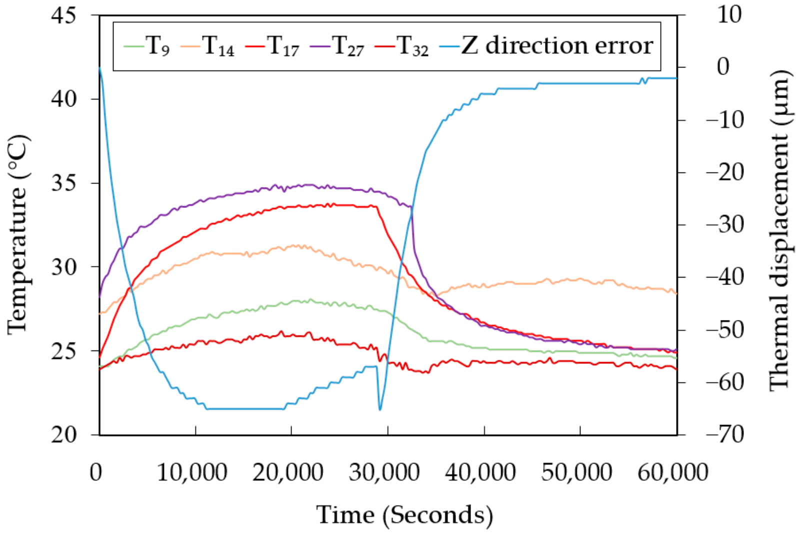

Figure 8. Trend analysis of five KTP temperatures and spindle displacement.

3.3. Model Establishment and Modeling Effect Comparison

To verify that the proposed LSTM modeling method could favorably estimate the spindle thermal displacement, the estimation effectiveness of the proposed model was compared with that of the MLR and BPNN models. The same five KTPs and the spindle speed S were used as the input, and spindle displacement in the z-direction was the output for the three modeling methods. Subsequently, three models of spindle displacement in the z-direction were separately established with the experimental data gathered at different spindle rotations. For the architecture of the ANN, the proposed LSTM and BPNN models were both set to have two hidden layers. Each of the two layers had ten hidden neurons, and the maximum training count was set to 100,000. The training curves of two modeling methods are shown in Figure 9. When the iteration number was 20,000, the proposed LSTM model was close to convergence with fewer errors than the BPNN. By contrast, the BPNN model approached convergence after 100,000 iterations.

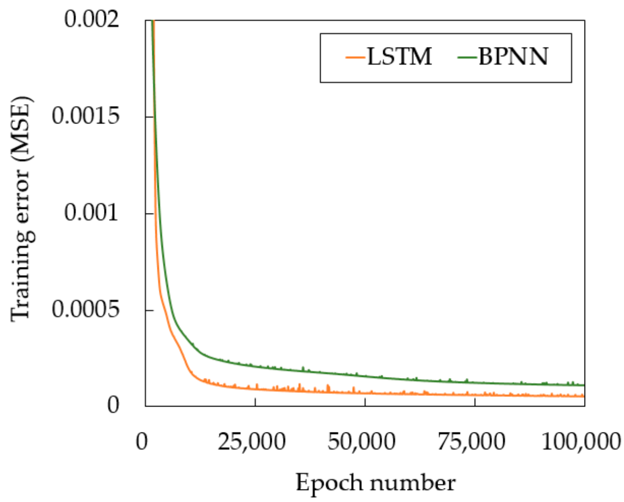

Figure 9. Training curve comparison between the proposed LSTM and BPNN models.

For the MLR modeling method, five KTPs and the spindle rotation speed S were the dependent variables, and the spindle thermal displacement in the z-direction was the independent variable. The best-fit coefficients between these independent and dependent variables were then obtained using the least squares method. The established MLR model is expressed in Equation (11).

$$Z = -0.93246\Delta T_{17} + 0.535236\Delta T_9 - 0.30063\Delta T_{27} - 0.18147\Delta T_{14} - 0.19361\Delta T_{32} - 0.01884S + 1.08416 \tag{11}$$

where ΔT_{17}, ΔT_9, ΔT_{27}, ΔT_{14}, and ΔT_{32} denote the temperature increase of the KTPs, and S is the spindle rotation speed. Figure 10 presents the results of the MLR, BPNN, and proposed LSTM models at different spindle rotation speeds. In the MLR modeling method, larger estimation errors occurred at the turning point of the spindle displacement curve (e.g., the estimation results at the 4th, 8th, and 12th hour). The largest estimated error reached 12.85 μm when the spindle rotation speed was 9000 rpm. The linear mathematical model is not enough to accurately describe the relationship between the temperature increase and spindle displacement. By contrast, the largest estimated errors for the BPNN and the proposed LSTM modeling methods were 6.96 and 3.22 μm, respectively. The ANN methods significantly outperformed the MLR modeling method. The proposed LSTM modeling method with memory characteristics had the best estimation performance at different spindle rotations.

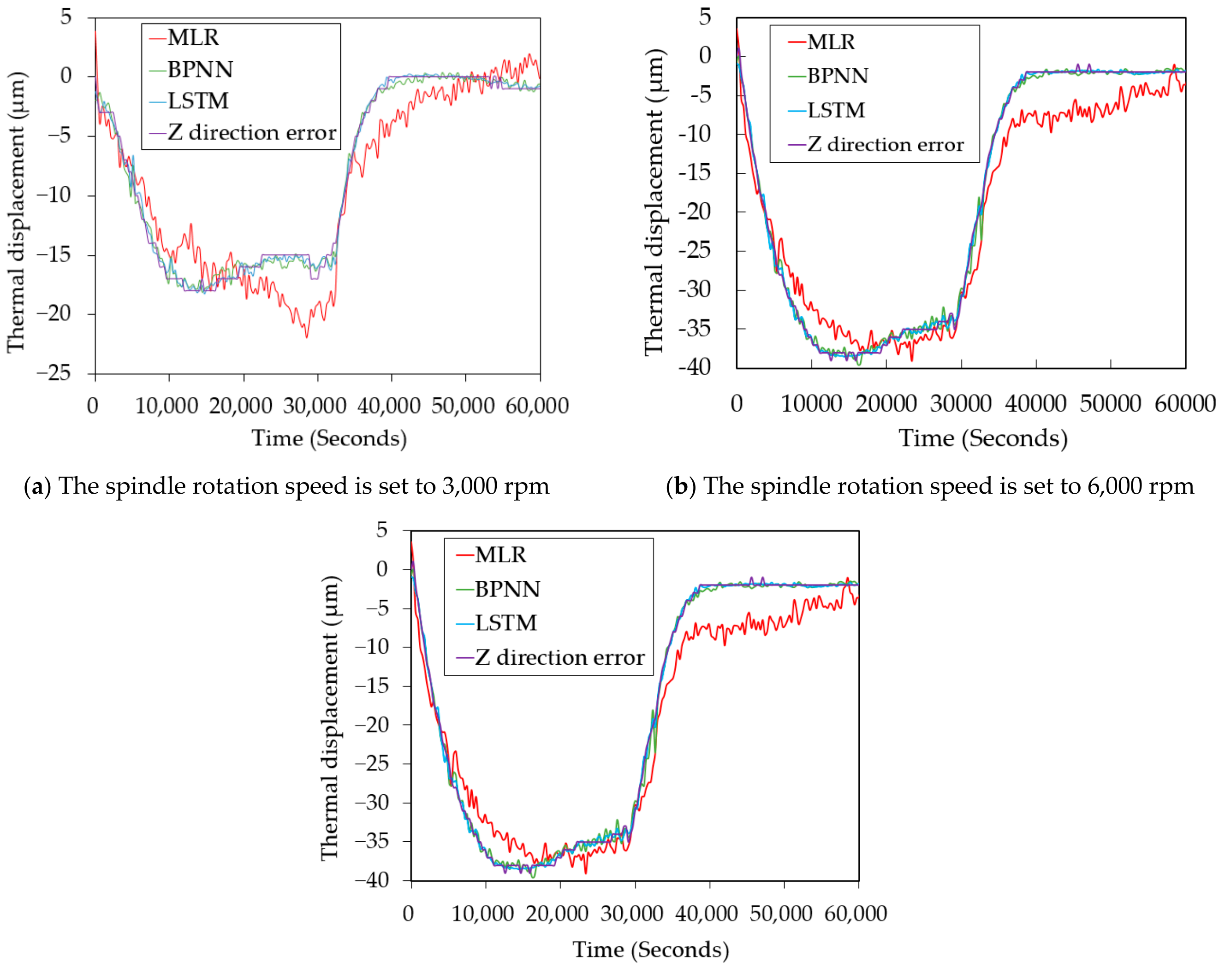

(**a**) The spindle rotation speed is set to 3,000 rpm (**b**) The spindle rotation speed is set to 6,000 rpm

(**c**) The spindle rotation speed is set to 9,000 rpm

Figure 10. Comparison estimation results of MLR, BPNN, and the proposed LSTM modeling methods at different spindle rotation speeds.

Table 8 presents the RMSEs of the MLR, BPNN, and the proposed LSTM modeling methods at different spindle rotation speeds. The three modeling methods exhibited a similar trend of more accurate estimations at low spindle speeds. The proposed LSTM modeling method consistently outperformed the MLR and BPNN methods in estimation for every spindle speed.

Table 8. RMSEs of the MLR, BPNN, and the proposed LSTM models at different spindle rotation speeds.

Spindle Speed	MLR	BPNN	LSTM
3000 rpm	2.716 μm	0.690 μm	0.529 μm
6000 rpm	3.792 μm	0.828 μm	0.554 μm
9000 rpm	4.966 μm	0.958 μm	0.625 μm

4. Conclusions

This study aimed to develop a robust and effective spindle thermal displacement modeling method to establish the relationship between the spindle thermal errors and the temperature changes. The selection of KTPs from the machine tool is important information that affects the performance of the prediction model and the cost of system implementation. The KTP selection method proposed to solve this problem removes the ITPs of invalid or highly identical features. The number of KTPs was reduced from 47 possible points to 5. Based on the proposed KTP selection scheme, three type of modeling methods, LSTM, MLR and BPNN, were discussed and compared. The results demonstrate that the performance of ANN-based modeling schemes (LSTM and BPNN) significantly outperformed the MLR modeling method, especially under a high rotation spindle speed. Different to BPNN, the proposed LSTM modeling scheme has a memory characteristic that can keep track of long-term dependencies in the input sequences. The experimental results demonstrate that the RMSE of the proposed LSTM is better than that of a BPNN at all spindle operating conditions. It proves the proposed LSTM is an ideal means of modeling temperature changes and spindle displacement.

The proposed spindle thermal error prediction scheme is verified at 3000, 6000, and 9000 rpm spindle rotation speeds. For the actual cutting state, more training data for modeling on different processing conditions, such as random spindle rotation speeds, need to be further considered and collected to simulate the actual cutting state, changes in temperature increases, and displacement of the spindle under different ambient temperatures. At the same time, the predicted effect of the machine tool in a real cutting stat also needs to be further studied.

Author Contributions: Conceptualization, Y.-C.L.; data curation, K.-Y.L.; investigation, K.-Y.L.; methodology, Y.-C.L.; project administration, Y.-C.L.; resources, Y.-C.L.; software, Y.-C.T.; validation, K.-Y.L.; visualization, Y.-C.T.; writing—original draft, Y.-C.T.; writing—review & editing, Y.-C.L.; All authors have read and agreed to the published version of the manuscript.

Funding: Please add: This research received no external funding.

Acknowledgments: This study was supported in part by grants from the Ministry of Science and Technology of the Republic of China (Taiwan) (Grant No. MOST 109-2221-E-167-014).

Conflicts of Interest: The authors declare no conflict of interest.

Appendix A

Table A1. Nomenclature used in this paper.

ITP	Initial Temperature Point.
KTP	Key Temperature Point.
BPNN	BackPropagation Neural Network.
RMSE	Root Mean Square Errors
ANN	Artificial Neural Network.
LSTM	Long Short-Term Memory.
MLR	Multiple Linear Regression.
RNN	Recurrent Neural Network
n	The number of ITPs.
ΔT	The temperature differences.
$\overline{T}$	The average of temperature.
C_Z	The correlation coefficient between ΔT of each ITP and the spindle displacement in the z-direction.
A	The number of data.
Z	The actual spindle displacement in the z-direction.
$\overline{Z}$	The average of spindle displacement in the z-direction.
y	The estimated output from the estimation model.
T_{b}	The reference point of the temperature rise.
T_s	The cluster centroid.
C_T	The correlation coefficient between T_s of cluster centroid and the other unclassified IPTs.
ρ	The clustering threshold.
v	The number of groups.
r	The number of KTP.
d_{max}, d_{min}	The maximum and minimum value in the specified data.
x_t	The LSTM unit input value of the t^{th} datum.
i_t, U^i, W^i, b^i	Denoted as the output, input weight, previous output weight, and bias of the input gate.
f_t, U^f, W^f, b^f	Denoted as the output, input weight, previous output weight, and bias of the forget gate.
o_t, U^o, W^o, b^o	Denoted as the output, input weight, previous output weight, and bias of the output gate.
$\widetilde{c}_t$	Denoted the current neural output.
U^g, W^g, b^g	Denoted as the output, input weight, previous output weight, and bias of the neural.
c_t	The memory cell output.
h_t	The LSTM unit output.

Table A2. The absolute Cartesian coordinates of all ITPs for experimental machine tool.

ITPs	Absolute Cartesian Coordinates (mm)	ITPs	Absolute Cartesian Coordinates (mm)	ITPs	Absolute Cartesian Coordinates (mm)
T_0	(0, 0, 0)	T_{16}	(140, −64, 260)	T_{32}	(0, 280, 270)
T_1	(−150, 269, 1040)	T_{17}	(140, 64, 420)	T_{33}	(0, −280, 270)
T_2	(−150, 269, 780)	T_{18}	(140, −64, 420)	T_{34}	(−716, −327, 1190)
T_3	(−111, −186, 1040)	T_{19}	(−616, 327, 840)	T_{35}	(−616, −780, 1080)
T_4	(−111, −186, 780)	T_{20}	(−616, 327, 600)	T_{36}	(−185, −554, 70)
T_5	(140, 0, 740)	T_{21}	(−616, 0, 840)	T_{37}	(−434, 455, 0)
T_6	(0, 140, 550)	T_{22}	(−616, 0, 600)	T_{38}	(−434, 686, 0)
T_7	(140, 0, 420)	T_{23}	(−616, −327, 840)	T_{39}	(−434, −686, 0)
T_8	(0, −140, 550)	T_{24}	(−616, −327, 600)	T_{40}	(−434, −455, 0)
T_9	(140, 0, 1180)	T_{25}	(−616, −764, 830)	T_{41}	(−388, −217, 580)
T_{10}	(0, 140, 1120)	T_{26}	(−616, −552, 610)	T_{42}	(−388, 0, 580)
T_{11}	(−180, 0, 1200)	T_{27}	(−616, −552, 300)	T_{43}	(−388, 217, 580)
T_{12}	(0, −140, 1120)	T_{28}	(−275, 556, 990)	T_{44}	(−265, 0, 580)
T_{13}	(140, 0, 190)	T_{29}	(−275, 0, 990)	T_{45}	(−265, 217, 580)
T_{14}	(140, 0, 1610)	T_{30}	(−275, −556, 990)	T_{46}	(1,000, 686, −180)
T_{15}	(140, 64, 260)	T_{31}	(−716, −327, 1560)	T_{47}	(140, −64, 380)

References

1. Bryan, J. International Status of Thermal Error Research. *CIRP Ann.* **1990**, *28*, 645–656. [CrossRef]
2. Mayr, J.; Jedrzejewski, J.; Uhlmann, E.; Donmez, M.A.; Knapp, W.; Hartig, F.; Wendt, K.; Moriwaki, T.; Shore, P.; Schmit, R.; et al. Thermal issues in machine tools. *CIRP Ann.* **2012**, *61*, 771–791. [CrossRef]
3. Postlethwaite, S.R.; Allen, J.P.; Ford, D.G. The use of thermal imaging, temperature and distortion models for machine tool thermal error reduction. *Proc. Inst. Mech. Eng.* **1998**, *212*, 671–679. [CrossRef]
4. Kim, H.S.; Jeong, K.S.; Lee, D.G. Design and manufacture of a three-axis ultra-precision CNC grinding machine. *J. Mater. Process. Technol.* **1997**, *71*, 258–266. [CrossRef]
5. Sugishita, H.; Nishiyama, H.; Nagayasu, O.; Shin-nou, T.; Sato, H.; O.-hori, M. Development of Concrete Machining Center and Identification of the Dynamic and the Thermal Structural Behavior. *CIRP Ann.* **1988**, *37*, 377–380. [CrossRef]
6. Spur, G.; Hoffmann, E.; Paluncic, Z.; Benzinger, K.; Nymoen, H. Thermal Behaviour Optimization of Machine Tools. *CIRP Ann.* **1988**, *37*, 401–405. [CrossRef]
7. Tanabe, I.; Takada, K.; Tsutsumi, M. Thermal deformation of machine tool structures using epoxy resin concrete. In Proceedings of the International Machine Tool Design and Research Conference, Manchester, UK, 17–18 September 1986; pp. 245–252.
8. Sun, L.; Ren, M.; Hong, H.; Yin, Y. Thermal error reduction based on thermodynamics structure optimization method for an ultra-precision machine tool. *Int. J. Adv. Manuf. Technol.* **2017**, *88*, 1267–1277. [CrossRef]
9. Li, K.Y.; Luo, W.J.; Wei, S.J. Machining Accuracy Enhancement of a Machine Tool by a Cooling Channel Design for a Built-in Spindle. *Appl. Sci.* **2020**, *10*, 3991. [CrossRef]
10. Mori, K.; Bergmann, B.; Kono, D.; Denkena, B.; Matsubara, A. Energy efficiency improvement of machine tool spindle cooling system with on–off control. *CIRP J. Manuf. Sci. Technol.* **2019**, *25*, 14–21. [CrossRef]
11. Shi, H.; He, B.; Yue, Y.; Min, C.; Mei, X. Cooling effect and temperature regulation of oil cooling system for ball screw feed drive system of precision machine tool. *Appl. Therm. Eng.* **2019**, *161*, 114150. [CrossRef]
12. Grama, S.N.; Badhe, A.N. A model-based cooling strategy for motorized spindle to reduce thermal errors. *Int. J. Mach. Tools Manuf.* **2018**, *132*, 3–16. [CrossRef]
13. Ramesh, R.; Mannan, M.A. Error compensation in machine tools—A review Part II. *Int. J. Mach. Tools Manuf.* **2000**, *40*, 1257–1284. [CrossRef]
14. Zhang, H.; Zhao, W.; Du, C.; Liu, H.; Zhang, J. Dynamic modeling and analysis for gantry-type machine tools considering the effect of axis coupling force on the slider–guide joints'stiffness. *Proc. Inst. Mech. Eng. Part B J. Eng. Manuf.* **2016**, *230*, 2036–2046. [CrossRef]
15. Shen, L.; Ding, X.; Li, T.; Kong, X.; Dong, X. Structural dynamic design optimization and experimental verification of a machine tool. *Int. J. Adv. Manuf. Technol.* **2019**, *104*, 3773–3786. [CrossRef]

16. Lv, Y.; Li, C.; Tang, Y.; Chen, X.; Zhao, X. Towards Lightweight Spindle of CNC Lathe Using Structural Optimization Design for Energy Saving. In Proceedings of the IEEE International Conference on Automation Science and Engineering (CASE), Hong Kong, China, 20–21 August 2020; pp. 220–225.
17. Li, Y.; Shi, H.; Ji, S.; Liang, F. Thermal Positioning Error Modeling of Servo Axis Based on Empirical Modeling Method. *Micromachines* **2021**, *12*, 201. [CrossRef]
18. Lin, C.J.; Su, X.Y.; Hu, C.H.; Jian, B.L.; Wu, L.W.; Yau, H.T. A Linear Regression Thermal Displacement Lathe Spindle Model. *Energies* **2020**, *13*, 949. [CrossRef]
19. Chen, T.C.; Chang, C.J.; Hung, J.P.; Lee, R.M.; Wang, C.C. Real-Time Compensation for Thermal Errors of the Milling Machine. *Appl. Sci.* **2016**, *6*, 101. [CrossRef]
20. Li, F.; Li, T.; Wang, H.; Jiang, Y. A Temperature Sensor Clustering Method for Thermal Error Modeling of Heavy Milling Machine Tools. *Appl. Sci.* **2017**, *7*, 82. [CrossRef]
21. Miao, E.; Liu, Y.; Liu, H.; Gao, Z.; Li, W. Study on the effects of changes in temperature-sensitive points on thermal error compensation model for CNC machine tool. *Int. J. Mach. Tools Manuf.* **2015**, *97*, 50–59. [CrossRef]
22. Liu, H.; Miao, E.; Wei, X.Y.; Zhuang, X.D. Robust modeling method for thermal error of CNC machine tools based on ridge regression algorithm. *Int. J. Mach. Tools Manuf.* **2017**, *113*, 35–48. [CrossRef]
23. Liu, H.; Miao, E.; Zhuang, X.; Wei, X. Thermal error robust modeling method for CNC machine tools based on a split unbiased estimation algorithm. *Int. J. Precis. Eng.* **2018**, *51*, 169–175. [CrossRef]
24. Pozevalkin, V.; Parfenov, V.; Polyakov, N. Approximation of machine tool experimental thermal characteristics by neural network. *J. Phys. Conf. Ser.* **2019**, 1–6. [CrossRef]
25. Jian, B.L.; Wang, C.C.; Hsieh, C.T.; Kuo, Y.P.; Houng, M.C.; Yau, H.T. Predicting spindle displacement caused by heat using the general regression neural network. *Int. J. Adv. Manuf. Technol.* **2019**, *104*, 4665–4674. [CrossRef]
26. Jian, B.L.; Guo, Y.S.; Hu, C.H.; Wu, L.W.; Yau, H.T. Prediction of Spindle Thermal Deformation and Displacement Using Back Propagation Neural Network. *Sens. Mater.* **2020**, *32*, 431–445. [CrossRef]
27. Reddy, T.N.; Shanmugaraj, V.; Vinod, P.; Krishna, S.G. Real-time Thermal Error Compensation Strategy for Precision Machine tools. *Mater. Today Proc.* **2020**, *22*, 2386–2396. [CrossRef]
28. Tian, Y.; Pan, G. An Unsupervised Regularization and Dropout based Deep Neural Network and Its Application for Thermal Error Prediction. *Appl. Sci.* **2020**, *10*, 2870. [CrossRef]
29. Yin, Q.; Tan, F.; Chen, H.; Yin, G. Spindle thermal error modeling based on selective ensemble BP neural networks. *Int. J. Adv. Manuf. Technol.* **2019**, *101*, 1699–1713. [CrossRef]
30. Zhou, Z.; Hu, J.; Liu, Q.; Lou, P.; Yan, J.; Hu, J.; Gui, L. The selection of key temperature measurement points for thermal error modeling of heavy-duty computer numerical control machine tools with density peaks clustering. *Adv. Mech. Eng.* **2019**, *11*, 1–11. [CrossRef]
31. Lou, P.; Liu, N.; Chen, Y.; Liu, Q.; Zhou, Z. The selection of key temperature measuring points for the compensation of thermal errors of CNC machining tools. *Int. J. Manuf. Res.* **2017**, *12*, 338–350. [CrossRef]
32. Abdulshahed, A.M.; Longstaff, A.P.; Fletcher, S. The application of ANFIS prediction models for thermal error compensation on CNC machine tools. *Appl. Soft Comput.* **2015**, *27*, 158–168. [CrossRef]
33. Kodinariya, T.M.; Makwana, P.R. Review on determining number of Cluster in K-Means Clustering. *Int. J. Adv. Res. Comput. Sci. Manag. Stud.* **2013**, *1*, 90–95.
34. ISO. *Test Code for Machine Tools-Part 3: Determination of Thermal Effects, Standard ISO/FDIS 230-3*; International Organization for Standardization: Geneva, Switzerland, 2001.
35. OMRON Corporation. Available online: https://automation.omron.com/en/us/products/family/ZX-E (accessed on 21 May 2021).
36. MST Corporation. Available online: http://teknikatools.myfactory.space/mk_urun_pdf/2017121391131.pdf (accessed on 20 May 2021).
37. Zhanga, C.; Gaoa, F.; Li, Y. Thermal error characteristic analysis and modeling for machine tools due to time varying environmental temperature. *Precis. Eng.* **2017**, *47*, 231–238. [CrossRef]
38. Li, Y.; Zhao, W.; Lan, S.; Ni, J.; Wu, W.; Lu, B. A review on spindle thermal error compensation in machine Tools. *Int. J. Mach. Tools Manuf.* **2015**, *95*, 20–38. [CrossRef]
39. Hochreiter, S.; Schmidhuber, J. Long short-term memory. *Neural Comput.* **1997**, *9*, 1735–1780. [CrossRef]